



HAL
open science

Effect of grain boundary planes on radiation-induced segregation (RIS) at near $\Sigma 3$ grain boundaries in Fe-Cr alloy under ion irradiation

Quentin Barres, Olivier Tissot, Estelle Meslin, Isabelle Mouton, Benoit Arnal, Marie Loyer-Prost, Cristelle Pareige

► To cite this version:

Quentin Barres, Olivier Tissot, Estelle Meslin, Isabelle Mouton, Benoit Arnal, et al.. Effect of grain boundary planes on radiation-induced segregation (RIS) at near $\Sigma 3$ grain boundaries in Fe-Cr alloy under ion irradiation. *Materials Characterization*, 2022, 184, pp.111676. 10.1016/j.matchar.2021.111676 . cea-03540781

HAL Id: cea-03540781

<https://cea.hal.science/cea-03540781>

Submitted on 24 Jan 2022

HAL is a multi-disciplinary open access archive for the deposit and dissemination of scientific research documents, whether they are published or not. The documents may come from teaching and research institutions in France or abroad, or from public or private research centers.

L'archive ouverte pluridisciplinaire **HAL**, est destinée au dépôt et à la diffusion de documents scientifiques de niveau recherche, publiés ou non, émanant des établissements d'enseignement et de recherche français ou étrangers, des laboratoires publics ou privés.



Distributed under a Creative Commons Attribution - NonCommercial - NoDerivatives 4.0 International License

Effect of grain boundary planes on radiation-induced segregation (RIS) at near $\Sigma 3$ grain boundaries in Fe-Cr alloy under ion irradiation

Q.Barrès^{a,c}, O.Tissot^a, E.Meslin^b, I.Mouton^a, B.Arnal^a, M. Loyer-Prost^b, C.Pareige^c

^a Université Paris-Saclay, CEA, Service de Recherches Métallurgiques Appliquées, 91191, Gif-sur-Yvette, France

^b Université Paris-Saclay, CEA, Service de Recherches de Métallurgie Physique, 91191, Gif-sur-Yvette, France

^c Normandie Univ, UNIROUEN, INSA Rouen, CNRS, Groupe de Physique des Matériaux, 76000, Rouen, France

email : olivier.tissot@cea.fr

Abstract : Due to their good mechanical properties and corrosion resistance, Ferritic Martensitic and ODS steels are widely studied for applications in the next generation of nuclear reactor. Under irradiation, migration of point defects leads to different mechanisms including radiation-induced segregation (RIS). This type of segregation affects defect sinks such as grain boundaries (GB). Many parameters influence the amplitude of the RIS such as temperature, dose and chemical composition of the alloy. This paper presents the quantification of GB plane variation on RIS. Two different near $\Sigma 3$ ($60^\circ \langle 111 \rangle$) GB were investigated using EBSD and TKD for structural characterization and APT and STEM/EDXS for chemical quantification. This work revealed W-shaped profiles of Cr across GBs and a heterogeneous precipitation of Cr-C rich particles in GBs planes after irradiation. Our work shows that not only the amplitude but also the sign of the Gibbsian Excess may be affected by the GB habit plane.

Key words: FeCr, atom probe tomography (APT), radiation-induced segregation (RIS), grain boundary, transmission kikuchi diffraction (TKD).

1 Introduction

For the next generation of reactor (GEN IV and Fusion), high Cr Ferritic Martensitic (F/M) steels and ODS alloys are potential candidates for structural and cladding applications due to their good mechanical properties such as a great swelling resistance under irradiation and corrosion resistance [1–3]. Irradiation defects created under irradiation (interstitials, vacancies, dislocation loops, voids) impact the microstructure evolution and the properties of these FeCr-based alloys. The diffusion of point defects (PD) in FeCr alloys may lead to α' precipitation [4–7] and intergranular segregation [8–10]. Radiation-Induced Segregation (RIS) can cause significant effects on materials, the local chromium composition may decrease until the alloy loses its stainless property or promote α' precipitation at the interface. For example, RIS can initiate irradiation-assisted stress corrosion cracking (IASCC) [11–13].

Two diffusion mechanisms drive RIS, inverse Kirkendall effect and the dragging effect. In the case of a Fe-Cr alloys, inverse Kirkendall effect leads to a depletion of chromium at sink by vacancy diffusion [14–18]. In the other hand, an attractive binding energy between interstitials and Cr atoms causes the formation of mixed dumbbells, which leads to an enrichment of sinks in Cr [16–24]. Segregation or depletion in Cr at sinks, like grain boundaries (GB), depends on many parameters. The occurrence of RIS as well as the preferred segregation mechanism are mainly related to the irradiation temperature and the dose rate used [25,26]. As mentioned by Lu et al. [27] there are many other parameters that can influence RIS occurrence and amplitude such as irradiation dose [10,26], grain size [28], solute element [29,30,26] and GB structure [31,32]. It is therefore difficult to anticipate a segregation trend under irradiation. Several studies have already been carried out as mentioned above, but few of them mention the influence of the nature of habit planes of the investigated GBs. This explains the need to

carry out analyses that try to isolate the impact of this variable on RIS. In literature, $\Sigma 3$ GBs are mainly known as “coherent twin” GB with low interface energy. But the definition of the coincidence site lattice (CSL) Σ^n does not fully define the structure of a GB as the nature of the planes at the GB are not taken into account. $\Sigma 3$ GB are not always twin [33]. In this study $\Sigma 3$ will have tilt and twist components which will be measured.

This paper reports on the quantification of segregation before and after Fe^{5+} ion irradiation at 450°C at 2 dpa on near $\Sigma 3$ GB in a Fe-13%Cr alloy using atom probe tomography (APT) and energy dispersive X-ray spectroscopy in scanning transmission electron microscope (EDS/STEM). These irradiation conditions were chosen, on the basis of the literature, in order to increase the dragging effect by interstitials and thus obtain an enrichment in Cr at GBs [26,34]. Two near $\Sigma 3$ GB with the same axe/misorientation angle ($60^\circ \langle 111 \rangle$) but different habit planes were investigated in order to study their influence on segregation. GB were fully characterized by their 5 degrees of freedom (5 DoF) thanks to Electron BackScatter Diffraction (EBSD) and transmission Kikuchi diffraction (TKD) orientation maps. Analyzes were conducted along the same GB before and after irradiation to quantify irradiation effects independently on the GB structure. In the first part, Materials and Methods are presented. In the second part, APT and STEM/EDS results are exposed and discussed.

2 Materials and methods

For this study, a high purity Fe-13Cr at.% alloy was analyzed. This alloy was produced at Ecole des Mines de Saint Etienne in France. It was prepared in an induction-melting furnace, formed with mechanical hammer at 1150°C and forged in a cold rolling machine (70% reduction). The alloy was heat treated for recrystallization for 1h at 1123 K under pure Argon flow followed by air-cooling at room temperature. The mean grain size is $363 \pm 161 \mu\text{m}$. The chemical composition of the alloy was obtained by APT analyses in the bulk of the alloy, results are given in the Table 1.

Table 1 : Bulk chemical composition of the Fe-13%Cr alloy by APT.

	Cr	O	N	C	Fe
wt. %	12.24	0.006	0.003	< 0.0002	Bal.
at. %	13.02	0.021	0.013	< 0.001	Bal.

Disc-like shaped samples of 100 μm in thickness and 3 mm in diameter were first mechanically polished from 320 to 1200 grid and then electro-chemically polished in a solution of 10% perchloric acid and 90% ethanol absolute ($T = -10^\circ\text{C}$, $V \approx 30 \text{ V}$) in order to remove plastic deformation introduced during mechanical polishing.

Irradiation was performed within the JANNuS-Saclay facility [35]. Fe-13at.% discs were irradiated with 5 MeV Fe^{5+} ions at $450 \pm 10^\circ\text{C}$. The temperature and the ions flux were measured all along the irradiation. Three thermocouples were in contact with the sample holder, another was welded on the back of one sample and an infrared camera was used for this irradiation. The measurement of the ions flux was ensured by 7 Faraday cages. Mean ions flux was $(2.1 \pm 0.5) \times 10^{11}$ ions/ cm^2/s during 8.3 hours of irradiation. Then damage and implantation profiles were calculated using SRIM-2008 [36] and IRADINA [37] with “Quick calculation of damage” mode in both cases. As shown in Figure 1 **Erreur ! Source du renvoi introuvable.**, IRADINA and SRIM-2008 calculations are in good agreement. A dose rate of 6.10^{-5} dpa. s^{-1} was calculated in the area of interest.

After irradiation, APT samples containing a GB at a depth of 300 nm were prepared in order to obtain an irradiation dose of around 2 dpa and to avoid the implantation peak.

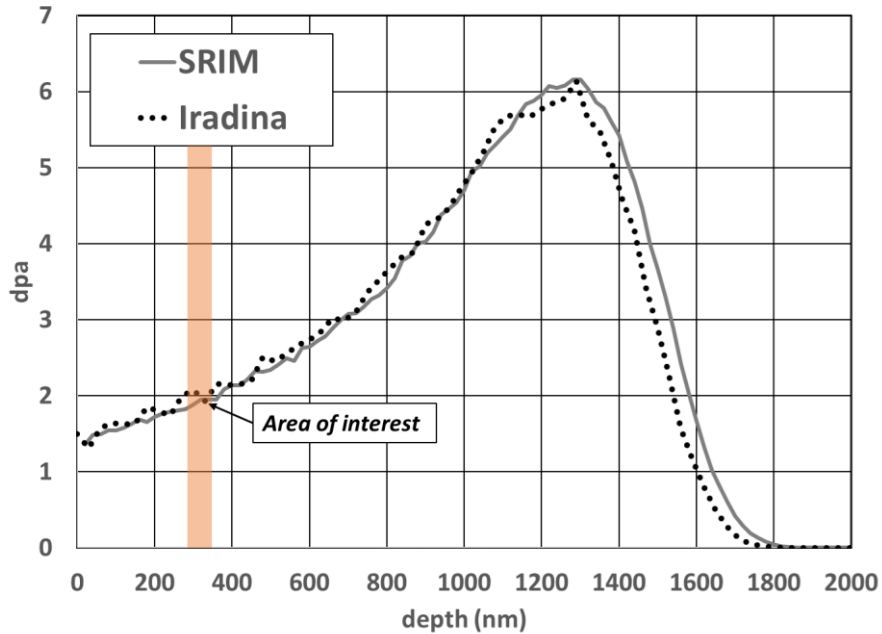


Figure 1 : Damage profile of 5 MeV Fe^{5+} irradiation at $6.10^{-5} \text{ dpa.s}^{-1}$ in a Fe-13%Cr comparing SRIM [36] and Iradina [37] results in "Quick calculation damage" mode.

EBSD mapping was performed on the surface of the sample to localize and identify GB (Figure 2.a). EBSD was used inside a scanning electron microscope - Focus Ion Beam (SEM-FIB) (Helios 650 NanoLab FEI) using a Bruker camera e-Flash HR and Esprit 2.1 software. The signal was obtained with an electron beam of 20 kV and 6.4 nA and a camera resolution of 160 x 120 pixels. Euler angles were treated with HKL Channel 5 (Oxford Instruments software) to obtain axe/angle of misorientation of each GB. To identify coincidence site lattice (CSL) GB [38] and avoid any misidentification of GB, several tests have been performed at different angular tolerances (5° , 2° , 1° , 0.5°). A tolerance value of 2° has been shown to be the most reliable criterion. This criterion avoids identification errors and is not too restrictive. Moreover, after each post-treatment, the misorientation of the identified near $\Sigma 3$ was verified by calculating the disorientation matrix from the Euler angles.

After identifying and selecting a specific GB, lift-out was performed along the GB (Figure 2.b). GB were also selected for their sub-surface orientation. Sub-surface escape angle between 25° and 60° (about 30° in Figure 2) allows the grain boundary to be intercepted at the correct depth during FIB milling. It also decreases the risk of sample failure during APT analysis and reduces the local magnification artefact on reconstruction. In order to compare exactly the same GB before and after irradiation, a 1st lift-out was extracted before irradiation along the GB of interest. After ion irradiation of the massive disc-shaped sample, the same GB was lifted out and APT and TEM specimens prepared (Figure 2.c). After several milling steps using FIB, when the APT sample diameter reaches 400-300 nm, TKD characterizations were performed. TKD characterization on an APT needle is already described in the literature [39–41]. In this study, TKD signal was obtained at a tilt angle of 52° with an electron beam of 30 kV and 13 nA. The camera resolution was also 160 x 120 pixels. The nature of the GB planes was determined using a stereographic projection created with CaRIne 3.1 software and based on TKD maps and Euler angles. Miller indexes were used to describe the crystallographic direction of the GB planes. In this study, their values of indexes (h,k,l) were rounded to a maximum value of 10 resulting in an uncertainty of 0.88° . To summarize, the five degrees of freedom of the GB were characterized [16,42] with both EBSD and TKD :

- Rotation axis: [hkl] (2 DoF),

- Misorientation angle : θ (1 DoF),
- GB plane orientation : $n_1 (h_{n1}, k_{n1}, l_{n1})$ and $n_2 (h_{n2}, k_{n2}, l_{n2})$ (2 DoF).

Those calculations were necessary to check GB structure inside each tip to ensure that segregation levels could be compared before and after irradiation independently of any structural effect.

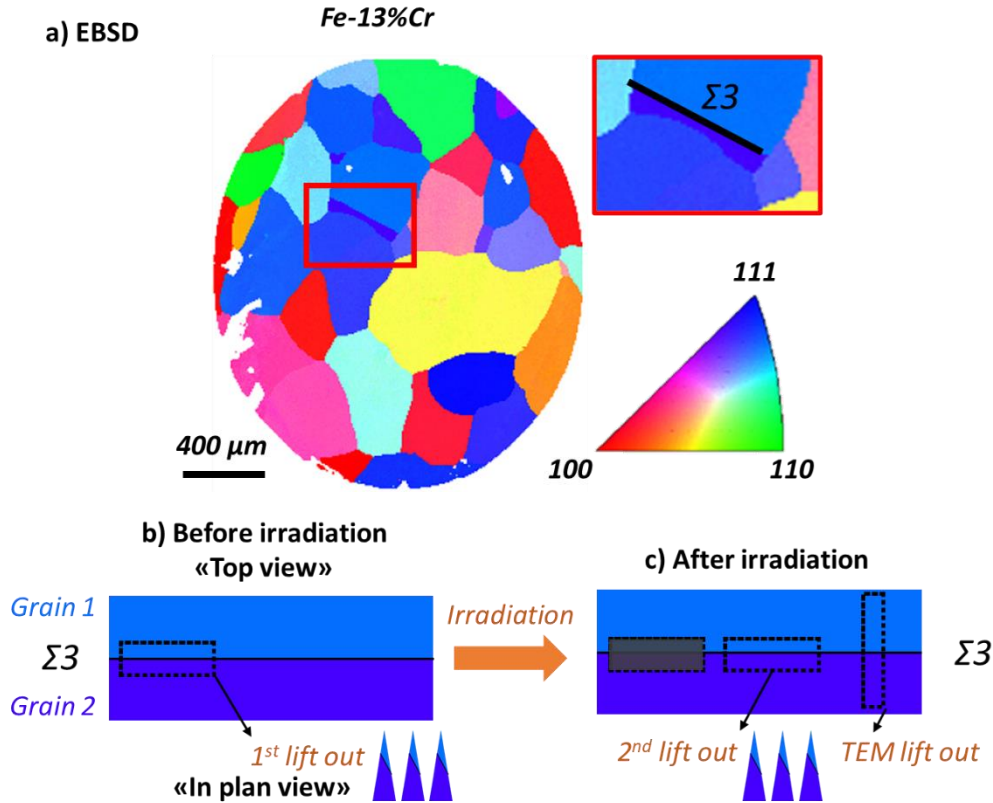


Figure 2 : Experimental protocol for GB identification by (a) EBSD then lift-out steps (b) before and (c) after irradiation using FIB.

APT tips were analyzed using a LEAP 4000X HR from CAMECA having a detector efficiency of 42%. Samples were cooled down to a temperature of 55K in order to avoid the preferential field evaporation of Cr atoms [43]. During analyses, the APT specimens were laser pulsed with an energy of 40 pJ, a pulse rate of 200 kHz and a detection rate of 0.003 atom per pulse. Reconstructions of the volumes were performed with IVAS 3.6.8 (CAMECA software) using spatial distribution map (SDM) on low index crystallographic poles to obtain reconstruction parameters (ICF = 1.65, β = 2.6). Composition profiles were performed across GBs to quantify segregation with a sampling step of 0.1 nm. Peak deconvolution was necessary at 27 Da due to the presence of both $^{54}\text{Fe}^{2+}$ et $^{54}\text{Cr}^{2+}$ isotopes. Concerning artefact due to the difference of evaporation field between Fe and Cr, Hatzoglou et al. show that the extent of this effect is less than the spatial resolution of the LEAP XHR < 1nm [44]. Composition peak on the GB plane and Gibbsian excess [45] were calculated to measure the magnitude of segregation or depletion on GBs. In order to obtain a better representativeness of the segregation at GB, APT analyses were doubled or tripled using two or three tips lift-out along the same GB.

After irradiation, TEM thin foils were also prepared with SEM/FIB to provide a quantitative estimate of the enrichment/depletion of Cr by energy-dispersive X-ray spectroscopy (EDXS). In this study, a probe-corrected FEI Titan 80-300 kV instrument operating at 300 kV has been used. EDXS measurements were performed with a Bruker Super-X four quadrant SDD detector for X-ray spectroscopy. The convergence angle was 22 mrad and the probe current and size were 100 pA and 1 nm respectively.

The lift-out of the cross-sectional thin foil has been performed at 90° of the GB trace (see Fig.2 (c)) to ensure that the GB is normal to the electron beam on the extracted thin foil. As a consequence, there is no need to tilt the thin foil during the EDXS measurements and the number of counts detected by the 4 detectors is the same. The quantification of the measurement has been done using the Cliff-Lorimer ratio technique [46]. Treatment of the data were performed with the Esprit 1.9 software.

3 Results

3.1 Crystallographic Structures

Two different near $\Sigma 3$ GBs were analyzed. This approach will allow to clearly isolate the effect of habit plane on RIS in the case of near $\Sigma 3$ GB structure. $\Sigma 3$ -1 and $\Sigma 3$ -2 were chosen for their subsurface orientation, between 30° and 60°, as well as their length, which help lift-out process. Their crystallographic structures are described in Table 2. The first near $\Sigma 3$ was characterized as $59.5^\circ[111](10,3,4)(-8,6,5)$. In the rest of the text, the reference “ $\Sigma 3$ -1” will be used for this GB. The second near $\Sigma 3$, called “ $\Sigma 3$ -2”, was described as $59.8^\circ[111](5,1,3)(-4,-5,2)$.

Table 2 : 5 DoF GB structure characterized by EBSD/TKD and the maximum of variations observed between APT samples coming from the same GB containing a near $\Sigma 3$ GB in Fe-13Cr.

	Structure					Max. Fluctuation		
	Θ/axe	n_1	n_2	Tilt angle	Twist angle	$\Delta\Theta$	Δn_1	Δn_2
$\Sigma 3$ -1	$59.5^\circ[111]$	(10.3.4)	($\bar{8}$.6.5)	29°	16°	0.7°	6.2°	4.2°
$\Sigma 3$ -2	$59.8^\circ[111]$	(5.1.3)	($\bar{4}$. $\bar{5}$.2)	40°	13°	0.5°	4.5°	4.9°

When crystallographic poles are visible in APT volumes, crystallographic orientation information can also be obtained via 2D density distribution of detector impacts (or desorption map). In Fe-13%Cr, low index poles are visible on density maps. This information can be compared to inverse pole figure (IPF) obtained in the same direction (APT analysis direction) with TKD. As illustrated in Figure 3, orientations deduced from IPF-Z maps obtained by TKD and the nearest low index poles extracted from APT density maps in each grain are in good agreement.

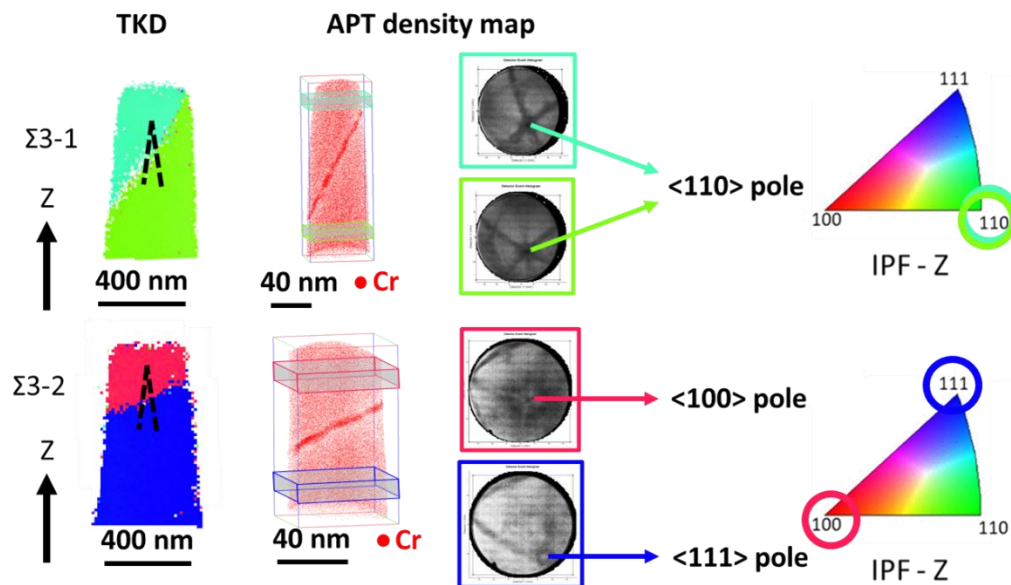


Figure 3 : Comparison between IPF-Z cartographies obtained by TKD and density maps extracted from each grain in APT reconstruction, for both GB, $\Sigma 3$ -1 and $\Sigma 3$ -2.

In order to control the reproducibility of the analyses, the variation of the orientation of the GBs in each APT specimen coming from the same lift-out were quantified (maximal fluctuation reported in Table 2). For both $\Sigma 3$, the maximal variation of the misorientation angle was 0.7° which is relatively low. The variation of the orientation of the normal of the GB planes was measured to be between 4.2° and 6.2° , this difference can be explained by the resolution of techniques used. EBSD and TKD techniques have a spatial resolution of several tens of nanometers and cannot give access to the atomic structure of the GB or the presence of facets [47]. The values measured are reasonably small to confirm that the same GB has been analyzed in each case either along one lift-out or between lift-outs extracted along the same GB.

3.2 $\Sigma 3$ before irradiation

In order to investigate the segregation level in the as-received state, samples from $\Sigma 3$ -1 and $\Sigma 3$ -2 before irradiation were analyzed with APT. An example of APT reconstruction for each kind of near $\Sigma 3$ is presented in Figure 4.a and c with a representative 1D composition profile of Cr and C drawn across the GBs of Figure 4.b and d. Profiles were performed with a section of $15 \times 20 \text{ nm}^2$ to analyze a large volume. To avoid artefacts, those volumes were made outside of crystallographic poles which are known to be enriched in Cr for some of them ((002) and (110)) [48].

The composition profiles and 3D images show that carbon atoms do not form any clusters or precipitates in the grains. The C profiles are noisy because the profiles have been drawn without any smoothing. In Figure 2b, C concentration appears larger in the second grain than in the first one. This is very likely an artefact links to the surface diffusion of C atoms under the electric field and the laser pulses towards some specific crystallographic sites. Depending on the orientation of each grain, the number of regions with a higher C concentration due to C surface diffusion may be different. This therefore may imply different apparent C concentration in the two grains. This effect is observed when C is in solid solution not in case of C segregation or when C forms clusters, precipitates.

Regarding Cr, the composition profiles reveal a Cr enrichment at the GBs. The profiles remain flat in the matrix of each grain showing the homogeneous distribution of Cr in grains. This has been confirmed by statistical tests. The maximum Cr concentration values and Gibbsian Excesses (Γ_{Cr}) [45,49] are listed in Table 3 for each sample. Results are similar for all samples with an average value of 20.9 at. %Cr at GB planes. We can also observe a variation from 18.46 %Cr to 26.59 %Cr in the $\Sigma 3$ -2 grain boundary. This deviation could be explained by the presence of intrinsic defects in the grain boundary. Gibbsian Excesses, although more dispersed, reflects a very local enrichment. A negative value reminds us how user-dependent are these measures, as Jenkins & al. had wisely pointed out [48]. In this study we estimate the uncertainty on Gibbsian Excesses to be about $2.0 \text{ at.}\cdot\text{nm}^{-1}$. Before irradiation, $\Sigma 3$ -1 and $\Sigma 3$ -2 GBs have a low level of chromium segregation. Besides, no other heterogeneity of composition was observed, such as α' phase, in or near GBs. The segregation levels observed before irradiation ($+5\% \leq \Delta \leq +13\%$) are in good agreement with previous results reported in the literature in Fe-6Cr, Fe-8Cr, Fe-15Cr alloys and a 16MnD5 steel [31,32,50,51]. In previous studies, Cr and other solute segregation levels were characterized. They showed that the amount of segregation was proportional to the initial composition and solubility limit of alloy elements. No heterogeneity was observed on or near these interfaces, except in the case of 16MnD5 steel, which has a more complex bainitic microstructure composed of laths of ferrite with the presence of carbides (such as cementite). This excess of solute elements observed before irradiation was caused by thermal segregation during the elaboration process.

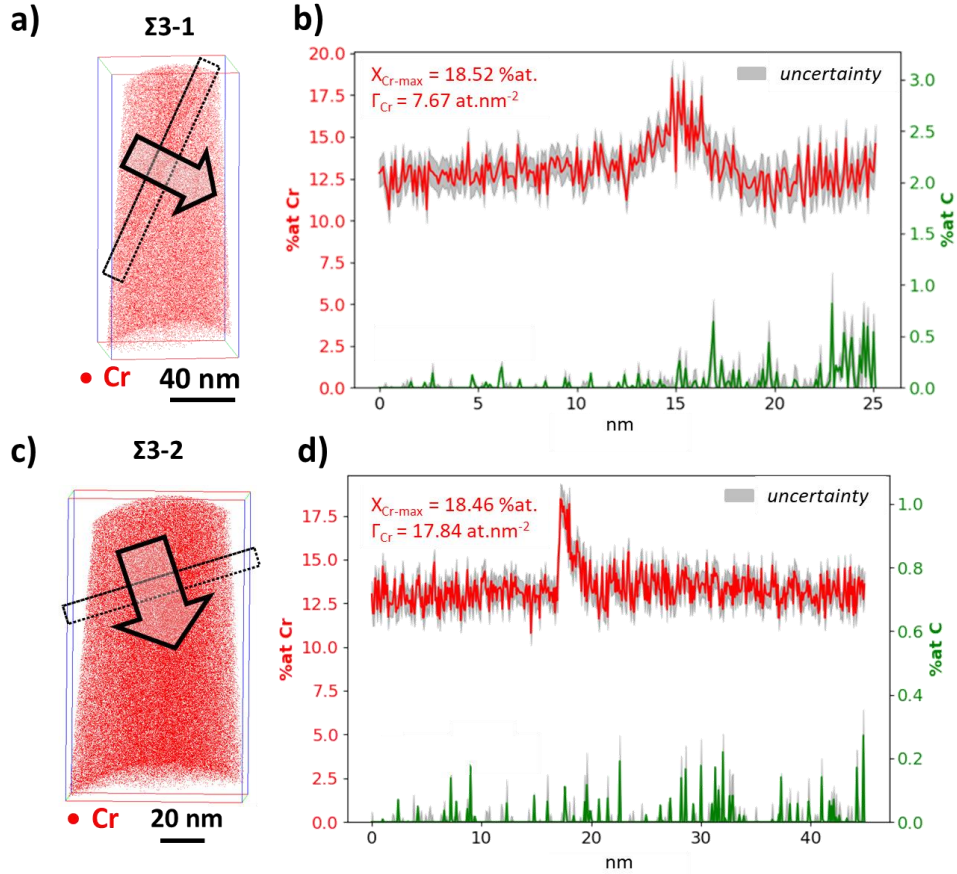


Figure 4 : Reconstructed APT volume showing the Cr distribution in the Fe-13%Cr before irradiation around GBs a) $\Sigma 3-1$ and c) $\Sigma 3-2$, the dotted rectangles delimit the GBs, and the black arrows represent the orientation of the composition profiles constructed perpendicularly to the GBs planes b) for $\Sigma 3-1$ and d) $\Sigma 3-2$.

Table 3 : Values of peak composition and Gibbsian excess of Cr for both near $\Sigma 3$ GBs before irradiation.

$\Sigma 3-1 N^\circ$	%Cr max	Γ_{Cr} (at.nm ⁻²)
1	18.52 ± 1.09	7.7
2	18.05 ± 1.21	3.9
$\Sigma 3-2 N^\circ$	%Cr max	Γ_{Cr} (at.nm ⁻²)
1	18.46 ± 0.88	17.8
2	22.84 ± 2.47	< -0.1
3	26.59 ± 3.36	10.9

3.3 $\Sigma 3$ after irradiation

Irradiations were carried out at 450°C with a dose rate of 6.10^{-5} dpa.s⁻¹ and samples were lifted-out at a depth of 300 nm to reach a dose of 2 dpa. For both near $\Sigma 3$ GBs, three samples were analyzed with APT. 1D-composition profiles were made across GB to compare results between APT and STEM/EDXS. All Cr profiles are characterized by a local enrichment on GB due to irradiation conditions which promote dragging effect of interstitials [26]. However, a second effect was also observed. A depleted area in Cr surrounds GBs over several tens of nanometers. This type of profile is known in irradiated steels as “W-shaped” profile [25,52–54]. One of the hypotheses put forward in the framework of austenitic steels to explain this W-shaped profile is the competition between segregation induced by irradiation and thermal segregation. Thermal segregation would tend to an enrichment of Cr at GB and the induced-segregation to a Cr depletion. The presence of carbon is also mentioned, the formation of

Cr-C complexes could fix chromium on GBs [34]. In our case, an enrichment in carbon coincides with the peak of chromium on GB in all analyzed tips after irradiation. This results are in agreement with previous studies for the formation of “W-shaped” on Cr profile associated with a peak of solute element [31,32]. In this non-equilibrium state, the annihilation of defects on GBs induces a peak of Cr enrichment in our case. A depletion zone is also visible around the grain boundary forming a W. The origin of this W-shaped profile is still discussed in the literature. The points frequently mentioned are the competition between irradiation-induced and thermal segregation and the effect of carbon [52,54]. Then, the extent of the depleted area could also be correlated with the sink strength of the GB and the sink density.

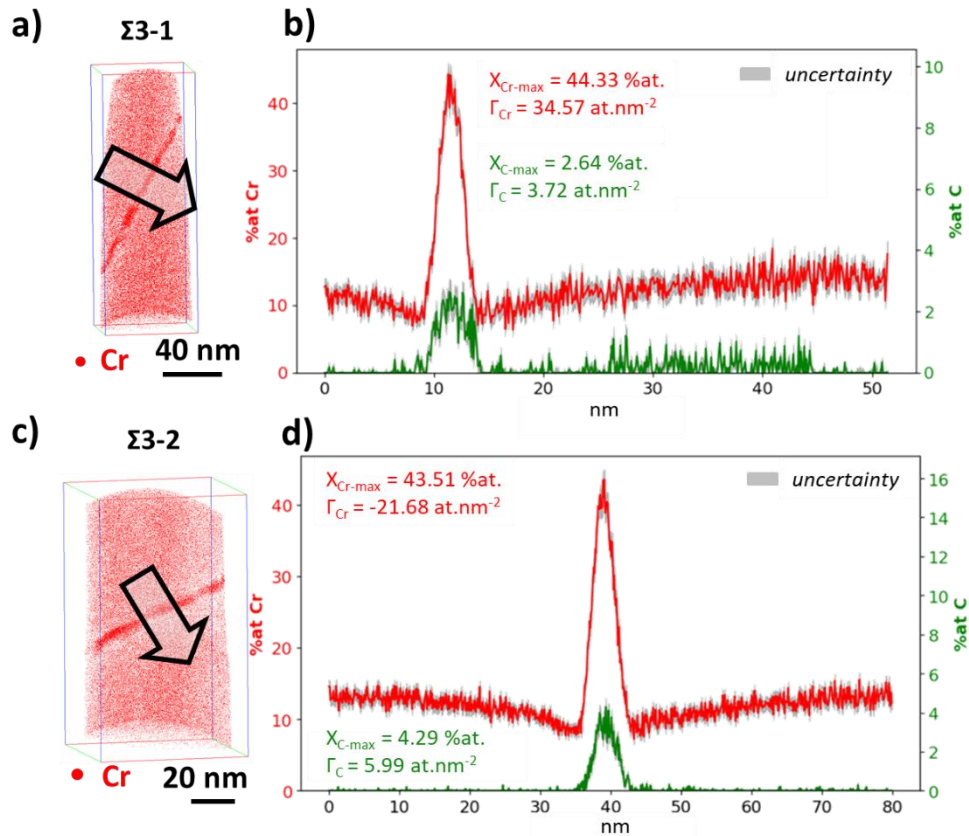


Figure 5 : Reconstructed APT volume showing the Cr distribution in the Fe-13%Cr after irradiation (450°C, 2 dpa) around GBs a) $\Sigma 3-1$ and c) $\Sigma 3-2$, the black arrows represent the orientation of the composition profiles constructed perpendicularly to the GBs planes b) for $\Sigma 3-1$ and d) $\Sigma 3-2$.

APT quantifications of Cr and C are summarized in Table 4. The average segregation level is about 42.04 at.%Cr and 2.98 at.%C for the $\Sigma 3-1$ and 40.42 %Cr and 4.42 %C for the $\Sigma 3-2$. It is important to note that a non-negligible amount of carbon was unwittingly added to the material during the irradiation and electron beam preparation steps. The main difference in the segregation behavior between these two near $\Sigma 3$ is highlighted by the gibbsian excess. In the first case, $\Sigma 3-1$, the gibbsian excess is positive and equal to about +41.0 at.nm⁻² in Cr whereas it is clearly negative for $\Sigma 3-2$ with about -30.0 at.nm⁻² in Cr. A negative excess means that chromium enrichment at the GB plane does not balance out the depletion around the GB. Which means that the GB and his surrounding area are globally depleted in chromium from a macroscopic point of view. The Gibbsian excess in carbon is quite similar for the two GBs. This variation of segregation levels between $\Sigma 3-1$ and $\Sigma 3-2$ could be attributed to GBs structure. According to the literature, it is known that the orientation of grain boundary plane has an effect on

the free volume of the interface and thus on its energy which can impact the sink strength and thus the segregation level [55,22,16].

After irradiation, STEM-EDX maps (Figure 6a and c) show periodic segregation in Cr along GBs and quantification profiles show a W-shaped profile in Cr in both cases. Those profiles confirm APT observations. Composition in Cr reach 23 and 24 at.% at GB after irradiation which is less than APT quantifications (Figure 6b and d). Coming from a non-irradiated zone after peak damage, those analyses did not report any Cr segregation at GBs.

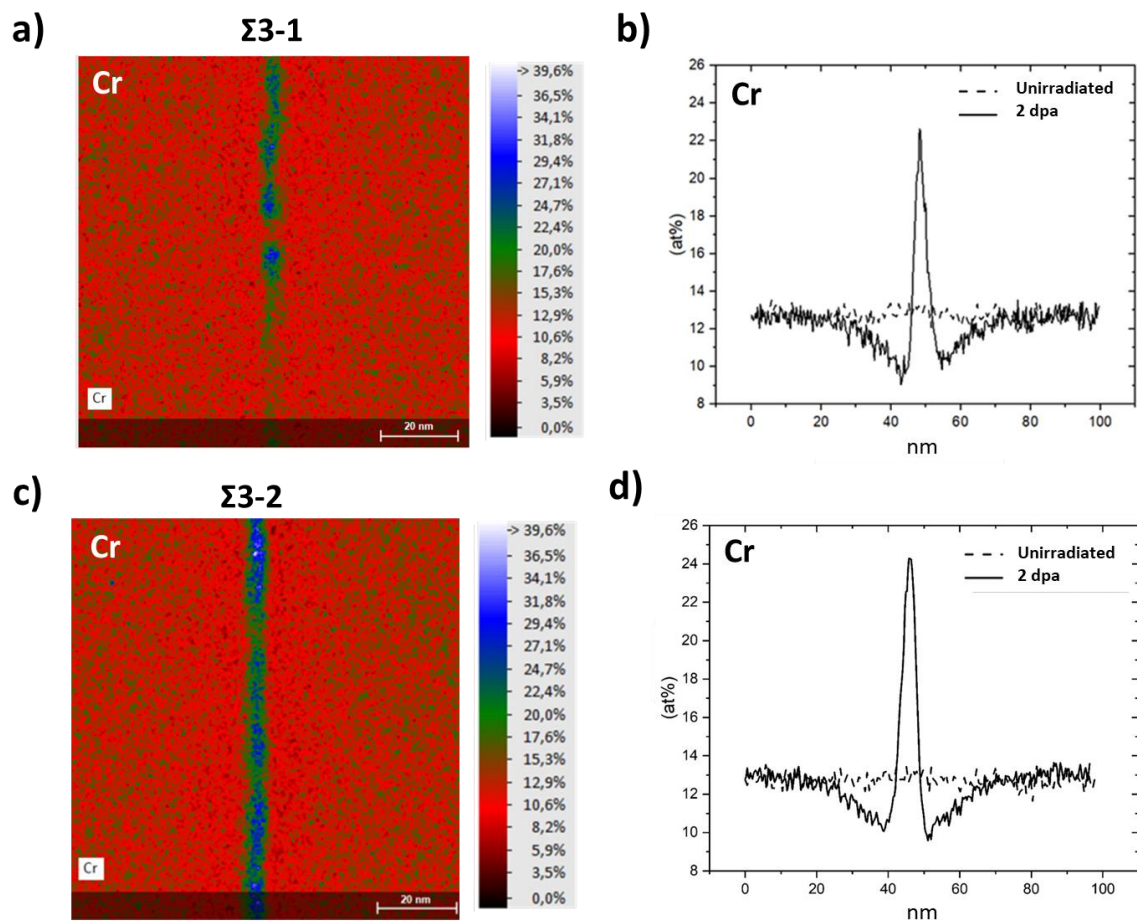


Figure 6 : EDXS map of Cr in the Fe-13%Cr after irradiation (450°C, 2 dpa) near GB a) Σ 3-1 and c) Σ 3-2; associated Cr-composition profiles obtained from EDX map for b) Σ 3-1 and d) Σ 3-2 (dotted line: far from irradiated area, solid line: at 2 dpa).

The difference of quantification between STEM-EDXS and APT is explained by the probe size and the moving step used. In STEM case, a probe size of 1 nm on a moving step of 0.58 nm was used, which implies an overlapping of the measurement points and a smoothing of the concentration values measured. In STEM, the entire thickness of the sample was probed for each a point of measurement and concentrations were averaged over the height, i.e. on 100 nm. For APT treatments, conditions were selected to not have overlap with a sampling box and moving step equal to 0.1 nm. Moreover, STEM probe size was ten times bigger than APT's, which dilutes the level of segregation obtained near the GB plane but STEM gave information's on a larger area, which shows the complementarity of these techniques.

Table 4 : Values of peak composition and Gibbsian excess of Cr and C for both GB near $\Sigma 3$ after 2 dpa at 450°C as measured with APT.

$\Sigma 3-1 N^\circ$	%Cr max	Γ_{Cr} (at.nm ⁻²)	%C max	Γ_C (at.nm ⁻²)
1	44.33 ± 2.64	34.6	2.64 ± 0.44	3.7
2	47.35 ± 2.64	44.9	3.80 ± 0.6	3.8
3	34.44 ± 1.49	43.4	2.51 ± 0.35	5.9
$\Sigma 3-2 N^\circ$	%Cr max	Γ_{Cr} (at.nm ⁻²)	%C max	Γ_C (at.nm ⁻²)
1	43.51 ± 1.41	-21.7	4.29 ± 0.47	6.0
2	43.0 ± 1.95	-29.8	5.66 ± 0.68	9.6
3	34.75 ± 1.92	-39.4	3.33 ± 0.55	4.4

One of the advantages of APT analyses is the 3D visualisation of the analyzed volume. In this case, it allows to observe more precisely the heterogeneities of the segregation in GBs planes. Using an iso-concentration tool, with a threshold value of 21 at. %, chromium-enriched particles are visualized in the plane of all near $\Sigma 3$ after irradiation (Figure 7.a). This threshold is the upper limit in Cr of a binomial distribution in a Fe-13%Cr [56]. This tool allows to visualize areas that have a composition beyond the statistical fluctuation of the matrix.

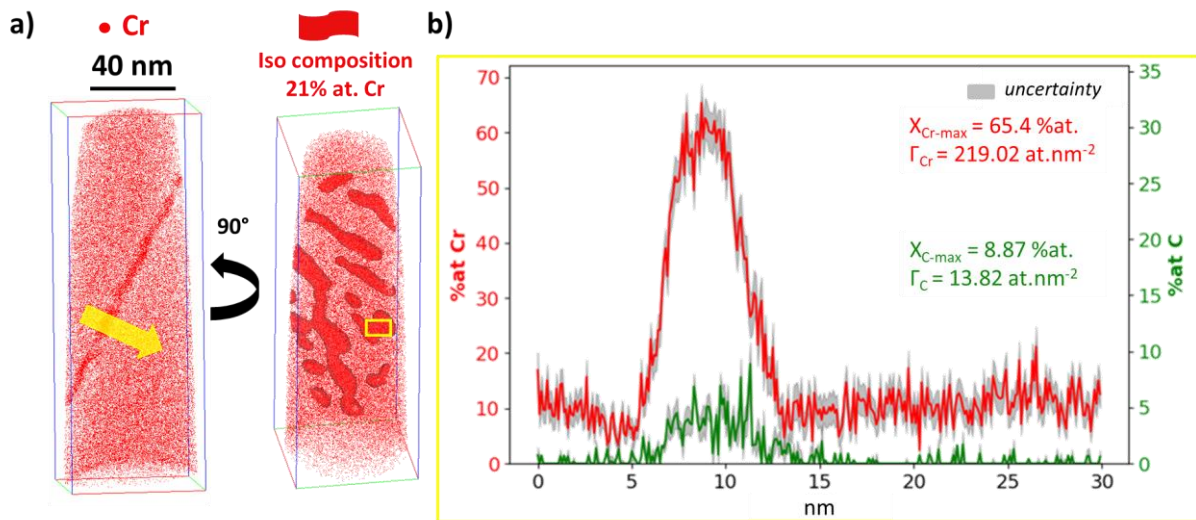


Figure 7 : a) Reconstructed APT volume showing the distribution of Cr (red) in Fe-13%Cr after irradiation (450°C at 2 dpa) in GB $\Sigma 3-1$ and an iso-concentration at 21 at. %Cr. The yellow arrow represents the composition profile obtained perpendicularly to GBs planes across a particle; b) composition profiles in Cr and C obtained.

By image processing using this threshold of 21 at. %, it has been determined that the distribution of particles in the plane covers randomly an area of about $(41 \pm 6) \%$. As showed by the composition profile in Figure 7.b, the composition of those particles can reach 65.4 at. %Cr and 8.87 at. %C. Three analyses in each near $\Sigma 3$ were performed to obtain more accurate results on these small objects. The average composition of the particles as measured in the two near $\Sigma 3$ GBs is reported Figure 8. One can note a difference in average composition of about 12.8 %Cr and 4.1 %C between the two GBs. Once again, the variation of GB energy induced by the difference of atomic arrangement between both GBs must impact post-irradiation segregation levels. However, the nature of these particles remains uncertain. There is too much carbon in these objects to be α' phase [6,4,57,5] and too less to be a

stoichiometric carbide. In this state, they can be considered as metastable carbide. The most common carbides found in these irradiated microstructures are $M_{23}C_6$ with a C/M ratio of 0.26 [27]. It should be emphasized that the only reference to intergranular precipitation after irradiation comes from Marquis et al. [58] who observed cubic carbides with an (Fe,Cr)/(C,N) ratio of 0.23 corresponding to $M_{23}(C,N)_6$ in a Fe15%Cr irradiated at a higher dose, 10 dpa at 300°C.

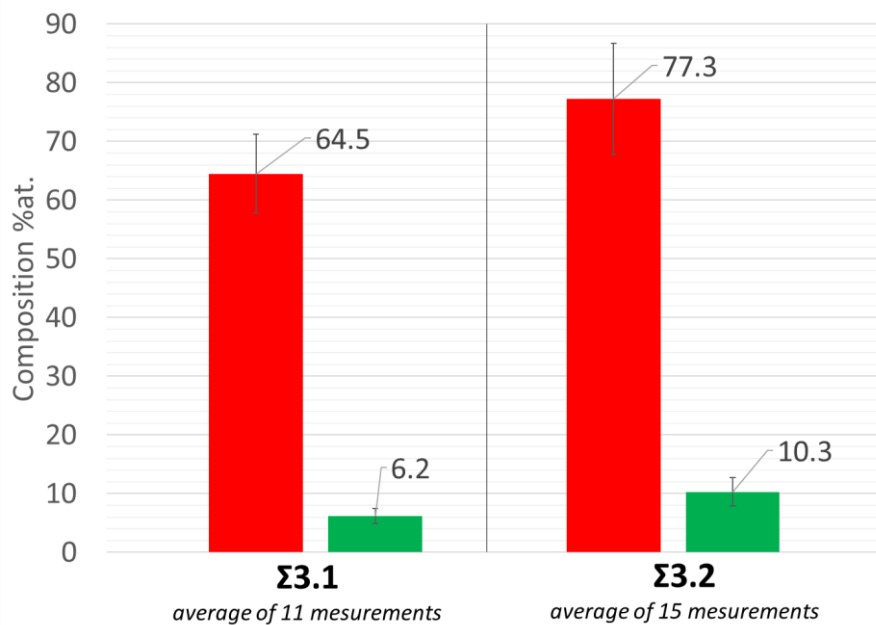


Figure 8 : Synthesis of chemical measurements of Cr-enriched particles in grain boundaries $\Sigma 3.1$ and $\Sigma 3.2$.

APT characterization of these chromium-enriched particles, randomly distributed in the GB plane, helps to explain the variations of Cr observed all along GB in STEM-EDX maps (Figure 6). These heterogeneities are difficult to observe in STEM, due to the projection of the GB on his whole thickness. It has been observed that the distribution in composition of those particles varies from one APT sample to another for a same GB (Figure 9). This difference could be attributed to a difference in the structure of the grain boundary at the nanometer scale, like facets, which may escape to EBSD/TKD characterization due to their limited spatial resolution or to the fact that these particles are not equilibrium phases. APT analyses are at local scale, which makes it impossible to see if other sinks are present near the GB. Competition between different sinks strength can lead to change segregation level locally.

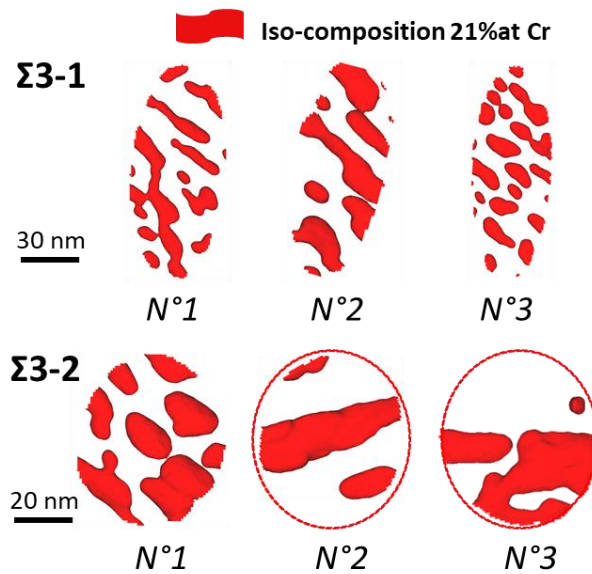


Figure 9 : Distribution of particles inside the plane of each GB $\Sigma 3-1$ and $\Sigma 3-2$ after irradiation (450°C, 2 dpa) in a Fe-13%Cr by iso-composition at 21 at. %Cr on APT reconstructed volumes.

Figure 10 presents composition profiles drawn in the GBs planes through the particles. These profiles show the abrupt interface between particles and their surrounding inside the GB plane. Between particles, a nearly constant Cr composition of 8 %Cr was measured in each APT sample for both near $\Sigma 3$ GBs. This low level of chromium concentration could be detrimental for material properties. Under 10% Cr, steels lose their stainless properties and corrosion can occur. Therefore, GB can be a place where corrosion will be initiated. In addition, the presence of particles in GBs plane can have an effect on the mechanical properties of this interface, leading to crack preferential initiation for example.

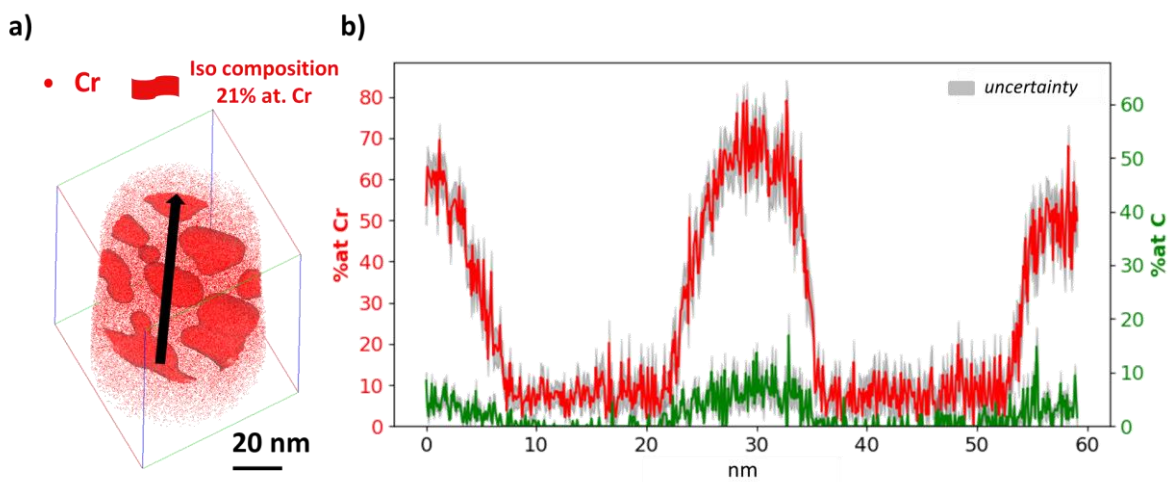


Figure 10 : a) Reconstructed APT maps facing the GB plane, showing the distribution of Cr (red) in Fe-13%Cr after irradiation (450°C 2 dpa) around GBs $\Sigma 3-1$ and an iso-composition surface at 21 at. %Cr, the black arrow represents composition profile obtained inside GB plane across several particles b) composition profiles in Cr and C following the arrow.

4 Conclusions

In this work, the effect of GB planes variation on segregation before and after ion irradiation (450°C, 2 dpa) was investigated, in a Fe-13 at.% Cr alloy. The specific experimental protocol used to prepare several tips along a same GB and the quantification of the segregation by APT

and STEM/EDXS analyses on two near $\Sigma 3$ GBs were presented. The main results of this investigation can be summarized as follow:

- Before irradiation, a low level of segregation was quantified reaching an average peak of composition on the GB plane about of 20.9 %Cr and 0.3 %C. This level of segregation is consistent with thermo-mechanical history of the alloy.
- After irradiation, a W-shaped profile of Cr is obtained with segregation of Cr and C at the GBs plane, as previously observed in the literature.
- Cr-C enriched particles are present in planes of both near $\Sigma 3$ GB after irradiation but the nature of these objects remains uncertain. It could be first steps of $M_{23}C_6$ carbide formation. Between particles, the composition of Cr decreases to reach a plateau equal to 8 %Cr that could initiate corrosion.
- The difference of plane orientation between both GB near $\Sigma 3$ have effects that were quantified. Gibbsian excess in chromium changes of sign from positive for $\Sigma 3.1$ with 41.0 at. nm^{-2} (3.4 monolayers) to negative for $\Sigma 3.2$ with $-30.0 \text{ at. nm}^{-2}$. The average composition in Cr and C of particles change between the two $\Sigma 3$, 64.5 %Cr / 6.2%C in the first case and 77.3 %Cr / 10.3 %C in the second case.

This study emphasizes the fact that the 5 DoF of GBs, the crystallographic structure of this interface, can affect GB response face to a stress such as RIS in this case. Moreover, the only measurement of the composition peak on GB plane do not allow to fully quantify the visible segregation after irradiation.

5 Acknowledgements

The experiments were done using JANNuS-Saclay (Joint Accelerators for Nanoscience and Nuclear Simulation). The technical staff of JANNuS-Saclay, CEA Paris-Saclay, France is greatly acknowledged for its support in performing irradiation experiments. The authors thanks Paul Haghi-Ashtiani from ECP for the help on the FEI Titan microscope.

This work received assistance from the “Agence Nationale de la Recherche” program GENESIS referenced as ANR-11-EQPX-0020 and from MATMECA consortium referenced as ANR-10-EQPX-37.

References

- [1] F.A. Garner, M.B. Toloczko, B.H. Sencer, Comparison of swelling and irradiation creep behavior of fcc-austenitic and bcc-ferritic/martensitic alloys at high neutron exposure, *Journal of Nuclear Materials*. 276 (2000) 123–142. [https://doi.org/10.1016/S0022-3115\(99\)00225-1](https://doi.org/10.1016/S0022-3115(99)00225-1).
- [2] R.L. Klueh, D.R. Harries, *High-Chromium Ferritic and Martensitic Steels for Nuclear Applications*, 2001.
- [3] P. Yvon, F. Carré, Structural materials challenges for advanced reactor systems, *Journal of Nuclear Materials*. 385 (2009) 217–222. <https://doi.org/10.1016/j.jnucmat.2008.11.026>.
- [4] V. Kuksenko, C. Pareige, P. Pareige, Cr precipitation in neutron irradiated industrial purity Fe–Cr model alloys, *Journal of Nuclear Materials*. 432 (2013) 160–165. <https://doi.org/10.1016/j.jnucmat.2012.07.021>.
- [5] M. Bachhav, G. Robert Odette, E.A. Marquis, α' precipitation in neutron-irradiated Fe–Cr alloys, *Scripta Materialia*. 74 (2014) 48–51. <https://doi.org/10.1016/j.scriptamat.2013.10.001>.
- [6] O. Tissot, C. Pareige, E. Meslin, B. Decamps, J. Henry, Kinetics of α' precipitation in an electron-irradiated Fe15Cr alloy, *Scripta Materialia*. 122 (2016) 31–35. <https://doi.org/10.1016/j.scriptamat.2016.05.021>.
- [7] O. Tissot, G. Sakr, C. Pareige, J. Henry, Effect of irradiation on nanoprecipitation in EM10 alloy - Comparison with Eurofer97, *Journal of Nuclear Materials*. 531 (2020) 151995. <https://doi.org/10.1016/j.jnucmat.2020.151995>.
- [8] S.M. Bruemmer, E.P. Simonen, P.M. Scott, P.L. Andresen, G.S. Was, J.L. Nelson, Radiation-induced material changes and susceptibility to intergranular failure of light-water-reactor core internals, *Journal of Nuclear Materials*. 274 (1999) 299–314. [https://doi.org/10.1016/S0022-3115\(99\)00075-6](https://doi.org/10.1016/S0022-3115(99)00075-6).
- [9] R.L. Klueh, D.R. Harries, *High-Chromium Ferritic and Martensitic Steels for Nuclear Applications*, 2001.
- [10] G.S. Was, J.P. Wharry, B. Frisbie, B.D. Wirth, D. Morgan, J.D. Tucker, T.R. Allen, Assessment of radiation-induced segregation mechanisms in austenitic and ferritic–martensitic alloys, *Journal of Nuclear Materials*. 411 (2011) 41–50. <https://doi.org/10.1016/j.jnucmat.2011.01.031>.
- [11] Z. Jiao, G.S. Was, Localized deformation and IASCC initiation in austenitic stainless steels, *Journal of Nuclear Materials*. 382 (2008) 203–209. <https://doi.org/10.1016/j.jnucmat.2008.08.032>.
- [12] Z. Jiao, G.S. Was, Impact of localized deformation on IASCC in austenitic stainless steels, *Journal of Nuclear Materials*. 408 (2011) 246–256. <https://doi.org/10.1016/j.jnucmat.2010.10.087>.
- [13] P.L. Andresen, G.S. Was, A historical perspective on understanding IASCC, *Journal of Nuclear Materials*. 517 (2019) 380–392. <https://doi.org/10.1016/j.jnucmat.2019.01.057>.
- [14] C.-C. Fu, Multiscale modelling of defect kinetics in irradiated iron, *nature materials*. 4 (2005). <https://www.nature.com/articles/nmat1286.pdf> (accessed July 16, 2018).
- [15] P. Olsson, C. Domain, J. Wallenius, Ab initio study of Cr interactions with point defects in bcc Fe, *Phys. Rev. B*. 75 (2007) 014110. <https://doi.org/10.1103/PhysRevB.75.014110>.
- [16] P. Lejcek, *Grain Boundary Segregation in Metals*, Springer, 2010.
- [17] J.P. Wharry, Z. Jiao, G.S. Was, Application of the inverse Kirkendall model of radiation-induced segregation to ferritic–martensitic alloys, *Journal of Nuclear Materials*. 425 (2012) 117–124. <https://doi.org/10.1016/j.jnucmat.2011.10.035>.
- [18] O. Senninger, F. Soisson, E. Martínez, M. Nastar, C.-C. Fu, Y. Bréchet, Modeling radiation induced segregation in iron–chromium alloys, *Acta Materialia*. 103 (2016) 1–11. <https://doi.org/10.1016/j.actamat.2015.09.058>.
- [19] P. Olsson, Ab initio study of interstitial migration in Fe–Cr alloys, *Journal of Nuclear Materials*. 386–388 (2009) 86–89. <https://doi.org/10.1016/j.jnucmat.2008.12.065>.
- [20] P.R. Okamoto, L.E. Rehn, Radiation-induced segregation in binary and ternary alloys, *Journal of Nuclear Materials*. 83 (1979) 2–23. [https://doi.org/10.1016/0022-3115\(79\)90587-7](https://doi.org/10.1016/0022-3115(79)90587-7).
- [21] D. Terentyev, P. Olsson, T.P.C. Klaver, L. Malerba, On the migration and trapping of single self-interstitial atoms in dilute and concentrated Fe–Cr alloys: Atomistic study and comparison with

- resistivity recovery experiments, *Computational Materials Science*. 43 (2008) 1183–1192. <https://doi.org/10.1016/j.commatsci.2008.03.013>.
- [22] M.A. Tschopp, K.N. Solanki, F. Gao, X. Sun, M.A. Khaleel, M.F. Horstemeyer, Probing grain boundary sink strength at the nanoscale: Energetics and length scales of vacancy and interstitial absorption by grain boundaries in alpha-Fe, *Phys. Rev. B*. 85 (2012) 064108. <https://doi.org/10.1103/PhysRevB.85.064108>.
- [23] J.P. Wharry, G.S. Was, The mechanism of radiation-induced segregation in ferritic–martensitic alloys, *Acta Materialia*. 65 (2014) 42–55. <https://doi.org/10.1016/j.actamat.2013.09.049>.
- [24] L. Messina, T. Schuler, M. Nastar, M.-C. Marinica, P. Olsson, Solute diffusion by self-interstitial defects and radiation-induced segregation in ferritic Fe–X (X=Cr, Cu, Mn, Ni, P, Si) dilute alloys, *Acta Materialia*. 191 (2020) 166–185. <https://doi.org/10.1016/j.actamat.2020.03.038>.
- [25] M. Nastar, F. Soisson, 1.18 - Radiation-Induced Segregation, in: R.J.M. Konings (Ed.), *Comprehensive Nuclear Materials*, Elsevier, Oxford, 2012: pp. 471–496. <https://doi.org/10.1016/B978-0-08-056033-5.00035-5>.
- [26] J.P. Wharry, G.S. Was, A systematic study of radiation-induced segregation in ferritic–martensitic alloys, *Journal of Nuclear Materials*. 442 (2013) 7–16. <https://doi.org/10.1016/j.jnucmat.2013.07.071>.
- [27] Z. Lu, R.G. Faulkner, G. Was, B.D. Wirth, Irradiation-induced grain boundary chromium microchemistry in high alloy ferritic steels, *Scripta Materialia*. 58 (2008) 878–881. <https://doi.org/10.1016/j.scriptamat.2008.01.004>.
- [28] E. Martínez, O. Senninger, A. Caro, F. Soisson, M. Nastar, B.P. Uberuaga, Role of Sink Density in Nonequilibrium Chemical Redistribution in Alloys, *Phys. Rev. Lett.* 120 (2018) 106101. <https://doi.org/10.1103/PhysRevLett.120.106101>.
- [29] T. Kato, H. Takahashi, S. Ohnuki, K. Nakata, J. Kuniya, The effect of solute content on grain boundary segregation in electron-irradiated Fe–Cr–Mn alloys, *Journal of Nuclear Materials*. 179–181 (1991) 623–625. [https://doi.org/10.1016/0022-3115\(91\)90165-4](https://doi.org/10.1016/0022-3115(91)90165-4).
- [30] Z. Lu, R.G. Faulkner, N. Sakaguchi, H. Kinoshita, H. Takahashi, P.E.J. Flewitt, Effect of hafnium on radiation-induced inter-granular segregation in ferritic steel, *Journal of Nuclear Materials*. 351 (2006) 155–161. <https://doi.org/10.1016/j.jnucmat.2006.02.026>.
- [31] R. Hu, G.D.W. Smith, E.A. Marquis, Effect of grain boundary orientation on radiation-induced segregation in a Fe–15.2at.% Cr alloy, *Acta Materialia*. 61 (2013) 3490–3498. <https://doi.org/10.1016/j.actamat.2013.02.043>.
- [32] M. Bachhav, L. Yao, G. Robert Odette, E.A. Marquis, Microstructural changes in a neutron-irradiated Fe–6at.%Cr alloy, *Journal of Nuclear Materials*. 453 (2014) 334–339. <https://doi.org/10.1016/j.jnucmat.2014.06.050>.
- [33] V. Randle, Role of grain boundary plane in grain boundary engineering, *Materials Science and Technology*. 26 (2010) 774–780. <https://doi.org/10.1179/026708309X12567268926641>.
- [34] M. Nastar, F. Soisson, 1.18 - Radiation-Induced Segregation, in: R.J.M. Konings (Ed.), *Comprehensive Nuclear Materials*, Elsevier, Oxford, 2012: pp. 471–496. <https://doi.org/10.1016/B978-0-08-056033-5.00035-5>.
- [35] A. Gentils, C. Cabet, Investigating radiation damage in nuclear energy materials using JANNuS multiple ion beams, *Nuclear Instruments and Methods in Physics Research Section B: Beam Interactions with Materials and Atoms*. 447 (2019) 107–112. <https://doi.org/10.1016/j.nimb.2019.03.039>.
- [36] J.F. Ziegler, M.D. Ziegler, J.P. Biersack, SRIM – The stopping and range of ions in matter (2010), *Nuclear Instruments and Methods in Physics Research Section B: Beam Interactions with Materials and Atoms*. 268 (2010) 1818–1823. <https://doi.org/10.1016/j.nimb.2010.02.091>.
- [37] J.-P. Crocombette, C. Van Wambeke, Quick calculation of damage for ion irradiation: implementation in Iradina and comparisons to SRIM, *EPJ Nuclear Sci. Technol.* 5 (2019) 7. <https://doi.org/10.1051/epjn/2019003>.
- [38] M. Mykura, *Grain Boundary Structure and Kinetics : a checkinst of Cubic Coincidence Site Lattice Relations*, Ed. R.W. Balluffi, Pub. ASM, Metals Park Ohio, 1980.

- [39] K. Babinsky, R. De Kloe, H. Clemens, S. Primig, A novel approach for site-specific atom probe specimen preparation by focused ion beam and transmission electron backscatter diffraction, *Ultramicroscopy*. 144 (2014) 9–18. <https://doi.org/10.1016/j.ultramicro.2014.04.003>.
- [40] K. Babinsky, W. Knabl, A. Lorich, R. De Kloe, H. Clemens, S. Primig, Grain boundary study of technically pure molybdenum by combining APT and TKD, *Ultramicroscopy*. 159 (2015) 445–451. <https://doi.org/10.1016/j.ultramicro.2015.05.014>.
- [41] B.M. Jenkins, J.O. Douglas, H.M. Gardner, D. Tweddle, A. Kareer, P.S. Karamched, N. Riddle, J.M. Hyde, P.A.J. Bagot, G.R. Odette, M.P. Moody, A more holistic characterisation of internal interfaces in a variety of materials via complementary use of transmission Kikuchi diffraction and Atom probe tomography, *Applied Surface Science*. 528 (2020) 147011. <https://doi.org/10.1016/j.apsusc.2020.147011>.
- [42] A.P. Sutton, R.W. Balluffi, *Interfaces In Crystalline Materials*, Clarendon Press Oxford, 1995.
- [43] O. Tissot, C. Pareige, E. Meslin, B. Décamps, J. Henry, Influence of injected interstitials on α' precipitation in Fe–Cr alloys under self-ion irradiation, *Materials Research Letters*. 5 (2017) 117–123. <https://doi.org/10.1080/21663831.2016.1230896>.
- [44] C. Hatzoglou, B. Radiguet, G. Da Costa, P. Pareige, M. Roussel, M. Hernandez-Mayoral, C. Pareige, Quantification of APT physical limitations on chemical composition of precipitates in Fe–Cr alloys, *Journal of Nuclear Materials*. 522 (2019) 64–73. <https://doi.org/10.1016/j.jnucmat.2019.05.022>.
- [45] B.W. Krakauer, D.N. Seidman, Absolute atomic-scale measurements of the Gibbsian interfacial excess of solute at internal interfaces, *Phys. Rev. B*. 48 (1993) 6724–6727. <https://doi.org/10.1103/PhysRevB.48.6724>.
- [46] G. Cliff, G.W. Lorimer, The quantitative analysis of thin specimens, *Journal of Microscopy*. 103 (1975) 203–207. <https://doi.org/10.1111/j.1365-2818.1975.tb03895.x>.
- [47] O. Hardouin Duparc, J.-P. Couzinié, J. Thibault-Pénisson, S. Lartigue-Korinek, B. Décamps, L. Priester, Atomic structures of symmetrical and asymmetrical facets in a near $\Sigma=9\{221\}$ tilt grain boundary in copper, *Acta Materialia*. 55 (2007) 1791–1800. <https://doi.org/10.1016/j.actamat.2006.10.041>.
- [48] B.M. Jenkins, F. Danoix, M. Gouné, P.A.J. Bagot, Z. Peng, M.P. Moody, B. Gault, Reflections on the Analysis of Interfaces and Grain Boundaries by Atom Probe Tomography, *Microscopy and Microanalysis*. 26 (2020) 247–257. <https://doi.org/10.1017/S1431927620000197>.
- [49] P. Maugis, K. Hoummada, A methodology for the measurement of the interfacial excess of solute at a grain boundary, *Scripta Materialia*. 120 (2016) 90–93. <https://doi.org/10.1016/j.scriptamat.2016.04.005>.
- [50] X. Zhou, X. Yu, T. Kaub, R.L. Martens, G.B. Thompson, Grain Boundary Specific Segregation in Nanocrystalline Fe(Cr), *Sci Rep*. 6 (2016) 34642. <https://doi.org/10.1038/srep34642>.
- [51] L. Zhang, B. Radiguet, P. Todeschini, C. Domain, Y. Shen, P. Pareige, Investigation of solute segregation behavior using a correlative EBSD/TKD/APT methodology in a 16MND5 weld, *Journal of Nuclear Materials*. 523 (2019) 434–443. <https://doi.org/10.1016/j.jnucmat.2019.06.002>.
- [52] M. Nastar *, Segregation at grain boundaries: from equilibrium to irradiation induced steady states, *Philosophical Magazine*. 85 (2005) 641–647. <https://doi.org/10.1080/14786430412331320035>.
- [53] E.A. Marquis, R. Hu, T. Rousseau, A systematic approach for the study of radiation-induced segregation/depletion at grain boundaries in steels, *Journal of Nuclear Materials*. 413 (2011) 1–4. <https://doi.org/10.1016/j.jnucmat.2011.03.023>.
- [54] R. Hu, G.D.W. Smith, E.A. Marquis, Effect of grain boundary orientation on radiation-induced segregation in a Fe–15.2at.% Cr alloy, *Acta Materialia*. 61 (2013) 3490–3498. <https://doi.org/10.1016/j.actamat.2013.02.043>.
- [55] M.A. Tschopp, D.L. McDowell, Structures and energies of $\Sigma 3$ asymmetric tilt grain boundaries in copper and aluminium, *Philosophical Magazine*. 87 (2007) 3147–3173. <https://doi.org/10.1080/14786430701255895>.
- [56] J.M. Hyde, G. DaCosta, C. Hatzoglou, H. Weekes, B. Radiguet, P.D. Styman, F. Vurpillot, C. Pareige, A. Etienne, G. Bonny, N. Castin, L. Malerba, P. Pareige, Analysis of Radiation Damage in Light

Water Reactors: Comparison of Cluster Analysis Methods for the Analysis of Atom Probe Data, Microscopy and Microanalysis. 23 (2017) 366–375. <https://doi.org/10.1017/S1431927616012678>.

- [57] V. Kuksenko, C. Pareige, C. Genevois, F. Cuvilly, M. Roussel, P. Pareige, Effect of neutron-irradiation on the microstructure of a Fe–12at.%Cr alloy, *Journal of Nuclear Materials*. 415 (2011) 61–66. <https://doi.org/10.1016/j.jnucmat.2011.05.042>.
- [58] E. Marquis, B. Wirth, G. Was, Characterization and Modeling of Grain Boundary Chemistry Evolution in Ferritic Steels under Irradiation, Univ. of Michigan, Ann Arbor, MI (United States), 2016. <https://doi.org/10.2172/1248953>.